SARS-CoV-2 and its variants, but not Omicron, induces severe thymic atrophy and impaired T cell development

Zaigham Rizvi
Translational Health Science and Technology Institute
Srikanth Sadhu
Translational Health Science and Technology Institute
Jyotsna Dandotiya
Translational Health Science and Technology Institute
Akshay Binayke
Translational Health Science and Technology Institute
Puja Sharma
Reginal Centre Biotechnology
Virendra Singha
Translational Health Science and Technology Institute
Vinayaka Das
Translational Health Science and Technology Institute
Ritika Khatri
Translational Health Science and Technology Institute
Rajesh Kumar
All India Institute of Medical Sciences
Sweety Samal
Translational Health Science and Technology Institute
Manjula Kalia
Regional Centre for Biotechnology
Amit Awasthi (aawasthi@thsti.res.in)
Translational Health Science and Technology Institute https://orcid.org/0000-0002-2563-1971

Article

Keywords: Thymic atrophy, SARS-CoV-2, Delta, Omicron, COVID-19, T cell development, IFNγ, double positive

Posted Date: May 5th, 2022

DOI: https://doi.org/10.21203/rs.3.rs-1581769/v1

Abstract

Pathogenic infections cause thymic atrophy, perturb thymic-T cell development and alter immunological response. Previous studies reported dysregulated T cell function and lymphopenia in coronavirus disease-19 (COVID-19) patients. However, immune-pathological changes, in the thymus, post severe acute respiratory syndrome coronavirus-2 (SARS-CoV-2) infection have not been elucidated. Here, we report SARS-CoV-2 infects thymocytes, depletes CD4 + CD8+ (double positive; DP) T cell population associated with an increased apoptosis of thymocytes, which leads to severe thymic atrophy in K18-hACE2-Tg mice. CD44 + CD25- T cells were found to be enriched in infected thymus, indicating an early arrest in the T cell developmental pathway. Further, Interferon gamma (IFN-γ) was crucial for thymic atrophy, as anti-IFN-g antibody neutralization rescued the loss of thymic involution. Therapeutic use of remdesivir (prototype anti-viral drug) was also able to rescue thymic atrophy. While Omicron variant of SARS-CoV2 caused marginal thymic atrophy, delta variant of SARS-CoV-2 exhibited most profound thymic atrophy characterized by severely depleted DP T cells. Recently characterized broadly SARS-CoV-2 neutralizing monoclonal antibody P4A2 was able to rescue thymic atrophy and restore thymic developmental pathway of T cells. Together, we provide the first report of SARS-CoV-2 associated thymic atrophy resulting from impaired T cell developmental pathway and also explains dysregulated T cell function in COVID-19.

Introduction

SARS-CoV-2 which was first reported in Wuhan, China in Dec, 2019 has so far infected around 6.3% of the total world population with around 1.23% mortality rate as on 18th April, 2022 (https://covid19.who.int/). Furthermore, emerging variants of concern (VoC) from the ancestral SARS-CoV-2 strain has led to sporadic emergence of COVID-19 related morbidity and mortality world-wide. While majority of clinical cases report pulmonary pathologies associated with pneumonia and acute respiratory distress syndrome (ARDS), growing number of evidences suggest cardiovascular, gastrointestinal, renal, neurological, endocrinological manifestations of SARS-CoV-2 infection [1–4]. Clinical cases of COVID-19 are also characterized by lymphopenia which is defined by T cell lymphodepletion [5]. Previous studies have shown that lymphopenia induced by pathogenic infection could be related to thymic atrophy [6–8].

Thymic atrophy is described as shrinking of the thymus and is related to aging or disease condition and leads to immuno-senescence (loss of T cell repertoire) and inflammaging (self-reactive T cell) (*6– 11*). Moreover, lymphopenia due to pathogenic infection could occur due to direct cellular killing induced by the pathogen or due to changes in the T cell developmental pathway in the thymus. Several mechanisms have been suggested for pathogen induced thymic atrophy which is governed by virus entry and infection. For example thymic atrophy by influenza A virus infection is mediated by IFN-γ cytokine or NK cells cytotoxicity and results in impaired negative selection [7,12]. For highly pathogenic avian influenza A virus (HPAIV), thymic atrophy occurs by impaired negative selection for T cells and involvement of glucocorticoids [13,14]. For chronic infection caused by hepatitis C virus, HIV infection, etc destruction of

thymus usually occurs through CD8 T cells and results in impaired negative selection [15,16]. Previous clinical post-mortem studies have suggested changes in the thymic structure which may be lead to changes in the thymic output post COVID-19 [6,11,17]. However, direct evidence of thymic atrophy and the mechanism involved in it have not been reported mostly due to lack of any animal model study. Golden Syrian hamster and humanized ACE2-transgenic mice are two routinely used models for SARS-CoV-2 infection which mimics upper and lower respiratory tract pathology. Interestingly, several reports have pointed that COVID-19 leads to extra-pulmonary pathologies ranging from gastrointestinal, cardiovascular, neurological, etc in both hamsters and hACE2 mice [18,19]. While hACE2 mice infected with SARS-CoV-2 develops acute COVID-19 and ultimately succumbs to infection, hamster represents a mild to moderate model for COVID-19 and have been shown to start recovering post day 6–7 of infection [19–22].

In the current study, we utilized golden Syrian hamster and hACE2 mice model for SARS-CoV-2 infection to investigate the cause of lymphopenia as seen in COVID-19 patients. We observed severe thymic atrophy in hACE2 mice infected with SARS-CoV-2. Immune profile of the thymocytes suggested skewed frequencies of DN and DP population and impaired T cell developmental pathway represented by changes in CD44 vs CD25 frequencies. The loss of T cells was found to be due to apoptosis and was mediated by IFN-γ as neutralization of IFN-γ abrogated thymic atrophy. Rescue of thymic atrophy was also observed with anti-viral drug remdesivir (RDV) which reduces viral load. Interestingly, infected hamsters do not develop severe thymic atrophy. Severe thymic atrophy was also absent from Omicron infection in hACE-Tg mice, however Delta variant infection seems to worsen thymic atrophy. Finally, we showed that P4A2 antibody, which has been recently reported as broadly SARS-CoV-2 neutralizing antibody effect against Delta variant, treated mice were rescued from thymic atrophy and showed no impaired T cell development. Together, we provide the first direct evidence of thymic atrophy induced by SARS-CoV-2 infection and show that the mechanism of thymic atrophy is through IFN-γ. Further, we show this impaired T cell development as a contributing factor for dysregulated peripheral T cell profile. Our results provide mechanism for the induction of lymphopenia and may explain waning T cell immunity post COVID-19 due to loss of TCR repertoire.

SARS-CoV-2 infection in hACE-2 mice causes lymphopenia. hACE2-transgenic (Tg) mice expressing humanized ACE2 receptor driven by epithelial cell cytokeratin-18 (K18) promoter had been shown as a model for acute model of SARS-CoV-2 infection following intranasal challenge with the live virus associated with rapid loss in body mass leading to mortality by day 6–8 post infection [22,23]. Consistent with the published reports, we found that hACE2-Tg mice infected with SARS-CoV-2 develops acute COVID-19 pathology characterized by sharp decline in body mass (Fig. 1A & 1B), 80% mortality by day 7 and profound presence of lung inflammation and injury as observed by assessing excised lung and hematoxylin and eosin (H&E) stained lung sections by trained pathologist (Fig. 1C- 1G). In line with this, there was profound localization of N protein in the infected lungs sections as determined by immunohistochemistry (IHC) corresponding to high N gene copy number (by qPCR) (Fig. 1H & 1I). Characteristic of the active infection, mRNA expression of anti-viral genes which are activated post sensing of viral RNA by toll-like receptors (TLRs) or rig-like receptor (RLRs) and activation of stimulator of

IFN genes (STING) such as 2'-5'-oligoadenylate synthetase (OAS)-2 and OAS-3, latent RNase (RNaseL), IFN-induced transmembrane (IFITM) protein, adenosine deaminase acting of RNA-1 (ADAR-1) [24] were all significantly increased in infected lung (Fig. 1J**).** Interestingly, the spleen and lymph node size of the infected mice at 6 dpi (peak of acute infection) showed profound involution with decrease in mass and live cell population (Fig. 1K-1O). Interestingly, we observed significantly reduced frequency as well as cell count of CD45.2+, CD3+, CD4 + and CD8 + lymphocytes in the splenocytes of the infected hACE2-Tg mice at 6 dpi as compared to uninfected mice (UI) (Fig. 1P-1Q). Curiously, there was a 3–4 folds upregulation in the frequency and count of DP cells in the splenocytes, which has been shown to be related to escape of DP cells from the thymus (Fig. 1P-1Q). Together, we found infected hACE2 mice manifests both pulmonary pathology as well as lymphopenia suggestive of dysregulated T cell development in the thymus.

SARS-CoV-2 infection induces thymic atrophy and leads to dysregulated T cell development. In line with the previously published reports, our clinical data showed a significant depletion of peripheral CD3 + and CD8 + T cells of COVID-19 patients as compared to the healthy control while a decreasing trend was observed for CD4 + T cells (Fig. 2A**)**. Changes in the thymus post-acute pathogenic infection have been previously shown to cause lymphopenia as thymus is the site of T cell development and maturation [7,8]. Emerging studies now show that lymphopenia is strongly correlated to morbidity and mortality and is associated with more than 50% of the adults and 10% of children infected with SARS-CoV-2 [25,26]. Lymphopenia is characterized by a substantial decrease in lymphocyte count and reduction in the frequency of peripheral CD4 + T helper and CD8 + T cytotoxic cells [26]. In line with this, the thymus of the infected hACE2-Tg mice at 6 dpi showed profound thymic involution (Fig. 2B & 2C**)** with a 7–8 folds decrease in mass and number of live cells (Fig. 2D). Next in order to understand the influence of SARS-CoV-2 infection on the thymic developmental pathway we looked at the virus entry and localization into the thymus. Our immunofluorescence data for SARS-CoV-2 specific anti-N protein localization indicated prominent presence of N protein in the thymocytes of the infected hACE2-Tg (Fig. 2E**)**. This was a surprising finding since no study has so far reported the expression of humanized ACE2 receptor in the thymus of hACE2-Tg mice. Since cellular injury of pulmonary and extra-pulmonary organs is characteristic pathological manifestation of COVID-19 and is often ascribed to the cellular entry and presence of virus, we evaluated the viral load in different compartments of thymocytes i.e. CD45+, CD45-, CD3+, CD3-, DP, DN cells in the sorted population (**Fig. S1A).** Our data shows presence of 2-2.5 log10 N gene copy number/ mg mass in all the compartments of thymocytes, suggesting that virus was able to internalize both in CD45- cells (which comprises of thymic epithelial cells) and CD45 + T cells with equal efficiency (Fig. 2F).

Next in order to understand whether virus induced thymic involution could result in dysregulation of T cell development we carried out a detailed immunophenotyping for different developmental stages of T cells in the thymus. We found a substantial increase in the frequency of CD45.2- cells, which was accompanied by expansion of CD45.2 + frequency in the infected thymus, however, there was a significant decrease in the cell count of both CD45.2 + and CD45.2- cells, suggesting that the depletion of

CD45.2 + cells were higher than that of CD45.2- cells though there was loss of both CD45.2 + and CD45.2- population due to viral infection (Fig. 2G & S1B). In line with this, we found 2 folds decrease in CD4 + CD8 + double positive (DP) and ~ 5 folds increase in CD4-CD8- double negative (DN) population with ~ 2–3 folds increase in single positive (SP) CD4 + or CD8 + cells indicating a profound dysregulation of T cell developmental pathway in infected thymus (Fig. 2H). Since dysregulated ratio of DP/DN was observed in thymus of infected mice, we made an attempt to understand at which developmental stage of triple negative (TN) population int the thymus is getting affected. Thymic development of TN occurs in 4 distinct stages viz CD44 + CD25- (DN1), CD44 + CD25+ (DN2), CD44-CD25+ (DN3) and CD44-CD25- (DN4) [7,15]. We found that thymus of the infected mice showed accumulated frequency for DN1 stage while a decrease in DN2 and DN3 percent frequency was observed for infected samples, suggesting an arrest at the early stage of T cell developmental pathway (Fig. 2I). We found ~ 4–6 folds increase in early and late apoptotic cells CD3 + thymocytes in infected as compared to the uninfected control (Fig. 2J). Similar trends in the induction of early and late apoptosis was found on CD45 + thymocytes, however CD45- thymocytes showed lesser frequency of apoptotic cells suggesting that CD3 + thymocytes are the major depleted population during SARS-CoV-2 infection in mice (**Fig S1C & S1D).** When time kinetics of infection pathology was studied to understand the early or late phase induction of thymic atrophy, we found that the degree of thymic atrophy was directly proportional to the severity of coronavirus disease-19 (COVID-19) with profound thymic atrophy at day 6 (but not day 3: I_3 post challenge) (**Fig S1E-S1J).**

Several mechanisms have been shown to influence thymic atrophy for pathogenic infection such as NK cells activation, increased levels of glucocorticoids as well as heightened IFN-γ secretion by the thymocytes. Previously studies have shown that pathogenic infections causes thymic atrophy associated with apoptosis of thymocytes which could be mediated by IFN-γ induced tissue injury [7,9,27]. Our data shows that SARS-CoV-2 infection results in profound elevation (~ 5 folds) of IFN-γ by CD45 + cells and to lesser extend (~ 2 fold) by CD45- cells (Fig. 2K & 2L). Moreover, SP CD8 + cells were found to be the major contributors of IFN-γ production in the thymus with ~ 6 fold upregulation during infection (Fig. 2M) which could be one of the driving factors for thymic atrophy as has been earlier reported [7]. Other pro-inflammatory cytokines such as Granzyme B (GzB), IL-4 and IL-17A was not found to be significantly altered, however interestingly, Perforin-1 (Prf-1) was found to be significantly up-regulated upon infection **(Fig. S1K-S1N)**. Together, we show that SARS-CoV-2 infection in hACE2-Tg mice results in thymic atrophy. Thymic atrophy was characterized by loss of DP population probably due to apoptosis and heightened IFN-γ which could be due to the persistence of virus in the thymus.

Neutralization of IFN-γ alleviates thymic atrophy induced by SARS-CoV-2 infection. IFN-γ, produced by both innate and adaptive arms of the immune system, has been earlier shown to be crucial mediator of inflammation and tissue injury during viral infections. Moreover, IFN-γ is critical in the induction of activation induced cell death (AICD) in T cells [28]. Elevated levels of IFN-γ was one of the key component of cytokine release syndrome in human and animal model [29]. In fact, our data indicate that a heightened IFN-γ levels in SARS-CoV2-infected hamster and K18-ACE2-Tg mice. In thymus, IFN-γ has been implicated in apoptosis of thymocytes resulting in tissue injury and thymic atrophy [7,10]. One previous study have

shown that thymic atrophy caused due to influenza A virus could be alleviated by neutralizing IFN-γ [30]. Since many aspects of pathogenesis and immunological response of influenza A virus and SARS-CoV-2 bear similarity, we speculated that IFN-γ could be one the key mediators of thymic atrophy for SARS-CoV-2 [31], and thus neutralize IFN-γ functions by using anti- IFN-γ neutralizing antibody. Anti-mouse IFN-γ neutralization was done one day prior and one day post SARS-CoV-2 infection in hACE2-Tg mice in order to neutralize the effector functions of IFN-γ induced upon SARS-CoV-2 infection (Fig. 3A). There was marginal protection in the body weight loss (**Fig S2A)** but no significant decrease in lung viral load in IFN-γ neutralized animals (**Fig S2B).** However, thymus of the animals receiving anti-IFN-γ antibody neutralization (I + IFN-γ) showed little or no signs of thymic involution in terms of size, mass and number when compared to the thymus from uninfected mice (Fig. 3B-3D). This corroborated with the decreased level of IFN-γ in animals receiving neutralizing antibody (Fig. 3E-3F). In line with the rescue of thymus size, the percentage frequency of CD45.2+/- cells were restored to normal levels as seen in uninfected control thymus (Fig. 3G). Moreover, the percentage frequency of DP and DN cells along with the percentage of DN1-DN4 population was also found to recover to their corresponding uninfected percentage frequency (Fig. 3H-3I). Finally, we showed that neutralization of IFN-γ effectively blunted the apoptosis of thymocytes, thus validating that the important and sufficient mediator of thymic atrophy in SARS-CoV-2 hACE2-Tg mice is IFN-γ (Fig. 3J**).** Since, SARS-CoV-2 in hACE2-Tg mice resulted in profound IFN-γ response, we asked whether IFN-γ induced tissue injury could also occur in C57BL/6 (WT) mice infected with SARS-CoV-2 without necessitating hACE2 receptor dependent virus entry. Remarkably, SARS-CoV-2 infected WT mice did not show any signs of pulmonary pathology or thymic involution as seen in hACE2 mice (**Fig S2C-S2L).** Together, our findings show that elevated IFN-γ secretion in SARS-CoV-2 infected hACE2-Tg mice leads to tissue inflammation and injury, thereby causing IFN-γ dependent thymic atrophy.

Use of remdesivir treatment reduces thymic viral load and rescues from thymic atrophy. In the beginning we described that SARS-CoV-2 infection through intranasal route results in virus entry and localization in the thymus. Presence of virus or viral factors have been shown to activate TLR3, TLR7 and TLR8 and RLR which leads to induction of anti-viral genes and cytokines characterized by heightened IFN-γ response [29,32]. This would mean that the use of anti-viral drugs which could reduce the viral burden and reduce viral antigens would also effectively reduce the inflammatory IFN-γ production and hence thymic atrophy. To test this, we used remdesivir (RDV, a prototypic anti-viral drug) which has been shown to have significant efficacy against SARS-CoV-2 infection in clinical cases [33,34]. Challenged animals receiving remdesivir (I + RDV) treatment significantly reduced lung viral loads and rescued mice from SARS-CoV2 induced pathologies (Fig. 4A, S2M-S2N). In line with this, RDV treatment in SARS-CoV2 infected mice significantly reduced thymic involution with size, mass and number of live thymocytes restored (approx.) to that of the uninfected animals (Fig. 4B-4D). Corresponding to this protection, there was profound reduction in the viral load throughout the thymus as assessed by immuno-fluorescence microscopy and qPCR (Fig. 4E-4F). In addition, animals receiving RDV treatment resulted in alleviation of thymic atrophy immune profile and rescued the normal developmental pathway of thymocytes with restored levels of CD45+/-, DP, DN cells (Fig. 4G-4H**).** In line with this, the developmental stages of DN population from DN1-

DN4 was restored back to their corresponding uninfected profiles (Fig. 4I). Next, we also evaluated the levels of IFN-γ and thymocytes apoptosis as it was important to understand whether RDV mediated rescue of thymic atrophy was operational through clearance of viral load from the thymus or it also resulted in blunted the inflammatory response and related thymic injury. IFN-γ response of CD45 + cells were reduced following RDV treatment and it also resulted in reduced percent frequency of thymocytes entering apoptosis which was expected as viral load and inflammation were earlier shown to be the driving factors for apoptosis of thymocytes (Fig. 4J-4L). Together, we show that reminiscent of IFN-γ, use of RDV (anti-viral drug) could effectively reduce the viral burden could rescue the thymic atrophy induced by SARS-CoV-2 infection.

In contrast to hACE2-Tg mice, golden Syrian hamster model mimics mild to moderate coronavirus disease-19 (COVID-19) as observed in majority of clinical cases [20]. In addition, we had earlier shown that the pulmonary pathology of coronavirus disease-19 (COVID-19) following SARS-CoV-2 infection in hamster peaks at 2–4 days post infection (dpi) with highest lung viral load, and starts to decline by 5–6 dpi with comparatively lower viral load and pulmonary pathology on 7 dpi [19]. Induction of thymic atrophy was evaluated at early and late phase in infected hamsters i.e. 4 and 7 dpi (**Fig S3A**). Though there was no significant difference in the size and mass of the excised thymus at 4 and 7 dpi as compared to that of 0 dpi thymus (**Fig S3B & S3C**), the number of live thymocytes as measured by trypan blue exclusion dye was significantly lower at 4 dpi (peak of infection) as compared to 0 dpi (uninfected) or 7 dpi (recovery phase of infection), suggesting signs of thymic injury at the peak of infection (**Fig S3D**). Thymus of the 4 dpi hamsters showed 100–500 copy number of viral gene N/ mg of thymus indicating thymic entry of SARS-CoV-2 (**Fig S3E**). We used anti-mouse CD4 (GK 1.5, cross reactive to hamster CD4) and anti-rat CD8 (cross reactive to hamster CD8) both having cross-reactivity with respective CD markers of hamster to study the development of T cells in thymus. Remarkably, we found 12–15% decrease in the DP cells at 4 dpi and 3–5% decrease in DN at 7 dpi as compared to the 0 dpi thymus DP cells. Similar dysregulated ratios were observed for SP CD4 and CD8 cells at 4 dpi. There was a sharp increase in DN cells at 4 dpi with approx. 2-fold increase as compared to 0 dpi thymus suggestive of dysregulated T cell development (**Fig S3F**). In line with this, we found 3–4 folds increase in early and late apoptotic cells at 4 dpi thymus accompanied with approx. 3 folds increase in thymic IFN-γ levels as compared to uninfected control (**Fig S3G & S3H**). Together, our findings show that acute COVID-19, but not moderate COVID-19 leads to severe thymic atrophy.

Delta variant, but not Omicron variant of SARS-CoV-2 induces severe thymic atrophy in hACE2 mice. The original Wuhan strain of SARS-CoV-2 (2019-nCoV) which caused first wave of pandemic in 2020 acquired continuous and considerable mutations in genetic material leading to antigenically different mutations which have been so far characterized into variants of concern (VoC), these VoCs lead to subsequent waves of pandemics across the globe or at different regions of the globe at different time points [35]. One such major VoC reported for SARS-CoV-2 was beta variant (B.1.351) that was first detected in South Africa with a large number of mutations in the spike region. The two other notable VoC appeared were Delta variant (B.1.617.2) first detected in India in late 2020 and recently reported omicron variant

(B.1.1.529) [36,37]. While both B.1.617.2 and B.1.1.529 have been shown to accumulate large amount of mutations in spike and receptor binding domain (RBD) and evade immune response, but only B.1.617.2 but not B.1.1.529 have been shown to cause severe COVID19 in hACE2-Tg animal model [38]. Since mutations reported in the VoC have been shown to evade immune response we became interested to investigate the effect of VoC challenge B.1.351, B.1.617.2 and B.1.1.529 on the induction of thymic atrophy (Fig. 5A). Consistent with the previously published reports, mice infected with variants except omicron showed rapid decrease in body mass and with presence of high N-gene copy number (**Fig S4A-S4B**). Our data demonstrate a most profound thymic atrophy in animals challenged with B.1.617.2 variant which closely mimicked the degree of thymic dysregulation of 2019-nCoV both in terms of involution of size, mass and thymocytes number. Interestingly, animals challenged with B.1.1.529 showed marginal thymic atrophy when compared to the original 2019-nCoV strain in line with the lower lung viral load **(**Fig. 5B-5D**)**. Consistent with the thymic atrophy we found significant VoC viral load in all the cellular compartment of thymus which was relatively lower for B.1.1.529 variant (Fig. 5E**)**. The profile of developing thymocytes as well as levels of IFN-γ secretion followed the pattern of infectivity with B.1.617.2 showing the highest while B.1.1.529 variant showing lowest dysregulation respectively when compared uninfected control (Fig. 5F-5J & S4C-S4G). Among the other pro-inflammatory cytokines only Prf-1 was found to be significantly elevated across VoC in CD4/CD8 thymocytes sub-sets (**Fig S4H-S4K).** Together, our data shows that among the 3 VoCs studies ie B.1.351, B.1.617.2 and B.1.1.529, B.1.617.2 (Delta) variants showed most profound thymic atrophy which was higher than that seen in the ancestral strain. While, B.1.1.529 showed milder induction of thymic atrophy.

P4A2 broadly neutralizing monoclonal antibody effectively reduced viral load and mitigated thymic atrophy. We previously demonstrated that the use of anti-viral drug RDV as an effective prophylactic treatment for rescuing thymic atrophy. We further investigated the therapeutic efficacy of P4A2, a murine monoclonal antibody broadly potent against VoC including Omicron by binding to the receptor binding motif (RBM) of SARS-CoV-2 RBD protein [39]. Monoclonal antibodies have previously shown to be effective in neutralizing SARS-CoV-2 in clinical settings and have the advantage of being administered as therapeutic dose post challenge even to immuno-compromised individuals [40]. We found effective neutralization of VoC and alleviation of thymic involution in mice receiving P4A2 antibody (Fig. 6A-D**)**. Likewise, the profile of the developing thymocytes along with the masking of IFN-γ secretion was also seen with the therapeutic dosing of P4A2 against all the VoC studied (Fig. 6E-6F**)**. Together, we show that the therapeutic dose of P4A2 antibody was effective and sufficient to neutralize VoC challenge and restore the thymic atrophy condition induced by SARS-CoV2 challenge.

Discussion

Researchers have so far described pulmonary and non-pulmonary pathologies arising due to COVID-19 in detail by using small animal model for SARS-CoV-2 infection. Several lines of evidences now suggest that the tissue injury as seen in the lungs or in case of multiple organ failure is attributed to dysregulated immune response [2, 41–44]. Clinical cases of COVID-19 are described by lymphopenia and cytokine release

syndrome (CRS) [5,25,29,45]. While CRS is known to be caused by strong pro-inflammatory response following SARS-CoV-2 infection, there is still lack of mechanistic evidence around the manifestation of lymphopenia. In the current study, we made an attempt to understand the mechanism involved in thymic atrophy as the reason behind lymphopenia in COVID-19 patients.

Thymus is a primary lymphoid organ and is the site of T cell developmental process which makes its role crucial in maintaining peripheral T cell frequency and function [46,47]. However, thymus health which is defined by thymic output is often modified by factors ranging from aging, pathogenic challenge, nutrition, transplantation, cancer and hormonal levels [48]. Thymic atrophy due to pathogenic infection could be attributed to changes in the precursor T cell entry or peripheral escape of thymocytes. In addition, thymic atrophy could also occur due to arrest in developmental pathway or increased apoptosis [10,13,46,47]. In line with this, we observed that hACE2-Tg mice infected with ancestral SARS-CoV-2 develops profound thymic involution with 7–8 folds reduced size. The cause of thymic atrophy was attributed to arrest of the developing thymocytes in the DN1 stage. Moreover, there was infection induced apoptosis of thymocytes leading to increased cell death. This was an interesting observation as till date no other report has shown infection induced thymic atrophy and subsequent loss of thymocytes due to apoptosis in case of COVID-19.

Increased cell death and impaired T cell development prompted us to investigate the mechanism of cell death and the role of virus or viral factors in promoting thymic atrophy. For this, we sorted different cell types of thymocytes and looked at the viral load. Surprisingly, our qPCR data shows presence of N gene RNA in all the cellular subsets of thymocytes. Though, we could find direct localization of virus in the cellular compartments of thymocytes both by qPCR as well as by fluorescence microscopy we still do not know what could be the exact mechanism of virus entry to the thymocytes whether the thymus infected progenitor T cells are migrating to the thymus thereby disseminating infection or whether virus is able to migrate to the thymus through direct sequestering. However quite remarkably we were able to find evidence that IFN-γ is not only crucial but also sufficient to induce thymic atrophy as neutralization of IFN-γ by neutralizing monoclonal antibody was able to rescue thymic atrophy completely. IFN-γ secreted in response to viral infection has been previously shown to be a mediator of tissue injury [7,14,28]. In addition to IFN-γ, pro-inflammatory cytokines such as IL17, IL4 and cytotoxic mediators such as Granzyme B and Perforin-1 have been previously reported to cause tissue injury and direct cell death [49–53]. We would that the frequency of none of these mediators, except Prf-1, was changed upon infection indicating that IL-17, IL-4, GzB, Prf-1 may have limited role in SARS-CoV-2 induced thymic atrophy. This was further validated by the IFN-γ neutralization experiment. Since presence of virus or viral factors was shown to induce IFN-γ response which was found to the culprit for thymic injury, we asked whether using an anti-viral drug which could remove the viral load could also mitigate thymic atrophy. Use of remdesivir as a treatment in hACE2 mice infected with SARS-CoV-2 effectively rescued mice from thymic atrophy. This could be because of the direct inhibition of virus and lack of activation of anti-viral response genes.

From the time of its origin in Wuhan, ancestral SARS-CoV-2 has gained substantial mutations which has been shown to escape immunity elicited by vaccinated candidates. Delta variant, which led to devastating causality world-wide have been especially shown to induce severe pulmonary pathologies [35–38, 54]. In line with this, our data shows that Delta variant, but not Omicron variant induced severe thymic atrophy which was worse than that induced by the ancestral strain. This was accompanied by profoundly impaired T cell development in Delta infected mice. Finally, we used a therapeutic intervention based on the use of monoclonal P4A2 neutralizing antibody to show that therapeutic intervention started at the early stages of infection could also help in the containment of thymic pathology and rescues the infected animal with restored T cell developmental pathway.

In summary, we present the first report of thymic atrophy induced by SARS-CoV-2 infection in both moderate and acute COVID19 model. Lymphopenia and immune dysregulation is a common feature of many pathogenic infection including influenza A and is influenced by the changes in the thymus. Moreover, thymus is the primary lymphoid organ and is central to the immune hemostasis. Through our study, we found that lymphopenia associated with SARS-CoV-2 infection could be attributed to thymic dysregulation and thymic atrophy. Since lymphopenia is known to persist long after COVID19 infection in clinical cases, we believe that thymic atrophy could be one of the important contributors of lymphopenia and may contribute to the alteration in peripheral T cell receptor repertoir. These findings may provide a paradigm change in our understanding of how immune-response (especially T cell response) is modulated during COVID-19 and may provide novel mechanism for designing vaccine candidates since thymic atrophy had been shown to result in loss of TCR repertoire.

Methods

Antibodies. Anti-mouse: α-CD45.2-APC-Cy7 (104, Biolegend, 1:700), α-CD3-BV510 (145-2C11, Biolegend, 1:700), α-CD4-PerCp (GK1.5, Biolegend, 1:1000), α-CD8-FITC or α-CD8-BV410 (53 – 6.7, Biolegend, 1:1000), α-IFN-γ-PE (XMG1.2, Biolegend, 1:500), α-IL17A-PE-Cy7 (TC11-18H10, Biolegend, 1:500), α-Perforin-APC (S16009A, Biolegend, 1:500), α-GzB-FITC (GB11, Biolegend, 1:500), α-IL-4-PE (11B11, Biolegend, 1:500), α-CD44-PECy7 (IM7, Biolegend, 1:600), α-CD25-PE (37C, Biolegend, 1:600), Annexin V-FITC (Biolegend, 1:400).

Animal Ethics and biosafety statement

K18-humanized ACE2 transgenic mice and C57BL/6 mice were initially obtained from Jackson laboratory, while golden Syrian hamster was procured from national institute of nutrition (NIN, India). Animals were housed and maintained in a conventional pathogen free environment at small animal facility (SAF) at Translational health science and technology institute (THSTI). The animals were maintained under 12 h light and dark cycle and fed a standard pellet diet and water ad libitum. Prior approval of the animal procedures was obtained from IAEC animal ethics committee (animal ethics approval number IAEC/THSTI/105 and IAEC/THSTI/151) and all the experimental procedures involving animals was done in accordance with the guidelines laid by institutional animal ethics committee of

THSTI. All experimental protocols involving the handling of virus cultures and animal infections were approved by RCGM, and the institutional biosafety and IAEC animal ethics committee.

Human Ethics:

Immunophenotyping of peripheral blood samples was performed according to the recommended guidelines of the Institutional Ethics Committee (Human Research) of THSTI and ESIC Hospital, Faridabad (Letter Ref No: THS 1.8.1/ (97) dated 07th July 2020). Human peripheral blood samples were collected from symptomatic COVID-19 patients and healthy participants after the written informed consent. Participants were enrolled in this study according to the inclusion/exclusion criteria set by the Institutional Ethics Committee (Human Research) of THSTI.

Virus preparation and determination of viral titers

SARS-Related Coronavirus 2, Isolate USA-WA1/2020, England VUI-202012/01 strain (NR-54000), SARS-CoV-2 (beta VoC), Isolate hCoV-19/USA/PHC658/2021 (Delta Variant) and SARS-CoV-2 B.1.1.529 variant (Omicron) virus was used as challenge strain and was grown and titrated in Vero E6 cell line grown in Dulbecco's Modified Eagle Medium (DMEM) complete media containing 4.5 g/L D-glucose, 100,000 U/L Penicillin-Streptomycin, 100 mg/L sodium pyruvate, 25mM HEPES and 2% FBS. The virus stocks were plaque purified and amplified at THSTI Infectious Disease Research Facility (Biosafety level 3 facility) as described previously.

SARS-CoV-2 infection

Infection in hamsters or hACE2-Tg transgenic mice was carried out as previously described [19,22]. The animals were briefly anesthetized through ketamine (100-150mg/kg) and xylazine (5-10mg/kg) intraperitoneal injections and thereafter the infection was established intranasally with 10^5 PFU (100 µl for hamsters and 50 µl for hACE2-Tg mice) of live SARS-CoV-2 or with DMEM mock control inside the ABSL3 facility. The remdesivir (RDV) group received a subcutaneous (sc) injection of remdesivir at 25 mg/kg body weight one day before infection and continued till day 3 post infection. Unchallenged animals received mock PBS injections on same time points.

IFN-γ neutralization

Neutralization of interferon gamma was carried out by anti-mouse IFNy antibody (XMG 1.2, BioXcell) 10 mg/Kg body mass 1 day prior to challenge and 2 days post challenge through intra-peritoneal injections. Control animals received mock control IgG antibody.

P4A2 treatment

Broadly SARS-CoV-2 neutralizing antibody P4A2 was given through intraperitoneal injection 4-6 h post challenge as previously described [39]. The unchallenged animals received non-specific IgG control antibody.

Clinical parameters of SARS-CoV-2 infection

All hamsters were housed for 4 and 7 days while mice were housed for approx. 6 days post challenge at ABSL3. Activity of the animals as well as their body mass was recorded daily post challenge. 6 animals from each group were sacrificed before mentioned end points and their blood serum along with body organs such as lungs, spleen, lymph nodes and thymus were collected. Serum samples were stored at -80 °C until further use. Lung, spleen, lymph nodes and thymus samples of challenged or unchallenged animals with or without treatment were compared for any gross morphological changes. Lungs samples were homogenized in 2 ml DMEM media and used for viral load and TCID50 determination. A section of the lung and intestine along with thymus section was fixed in 10% formalin solution and used for H & E staining and immuno-fluorescence microscopy. Spleen and thymus were strained through 40 µm cell strainer with the help of a syringe plunger and used for immunophenotyping and qPCR. Number of live cells from thymus and lymph node was determined by trypan-blue exclusion method.

Cell sorting

Thymus of the euthanized animals at end point were used to prepare single cell suspension and then surface stained with anti-mouse: α-CD45.2-APC-Cy7, α-CD3-BV510, α-CD4-PerCp, α-CD8-FITC antibodies. Cells were then washed with 1X PBS and sorted on BD FACS Aria III with approximately >98% purity.

Immunophenotyping of Human PBMCs:

Blood samples were collected from COVID-19 patients [n=18; median age 26.5 years (IQR 24:34.5)] within 0-4 days of PCR positivity. Similarly, blood was collected from age-matched RT-PCR negative, healthy individuals [n=18; median age 27.5 years (IQR 25:32y)]. Peripheral blood was drawn in Sodium Heparin CPT^{TM} tubes and the tubes were centrifuged at 1500g for 25 min. The PBMCs were separated, washed twice and cryopreserved until further use. The frozen PBMCs were thawed and rested in complete media as described previously [55]. To calculate the frequency of T cells, the cells were were stained for viability and surface markers (CD3 BV785, 1:100; CD4 FITC, 1:100; CD8 BV510, 1:100, all Biolegend USA) in FACS buffer (PBS supplemented with 2% FBS (Gibco)) for 40 min at 4 °C. Next, cells were fixed using the Cytofix/Cytoperm kit (BD Biosciences) and acquired on BD FACSymphony^{TM} instrument (BD Biosciences) using BD FACSuite software (V1.0.6) and analyzed with FlowJo VX (FlowJo LLC, BD Biosciences). The data representation and statistical analysis was performed using GraphPad Prism 9.0.

Flow cytometry and intracellular cytokine staining

Processed cells from spleen or thymus were stained for surface markers by using FACS antibodies in FACS buffer (PBS with 1% FBS) as previously described [56]. Briefly, cells were stimulated with phorbol 12-myristate13-aceate (PMA; 50 ng/ml; Sigma-Aldrich) and ionomycin (1 µg/ml; Sigma-Aldrich) for 4 h in presence of Monensin (#554724 Golgi-Stop, BD Biosciences). Thereafter, cells were washed and incubated with Fc block (anti-mouse CD16/32, Biolegend) at room temperature (RT) for 20 min followed by surface staining with α-CD45.2, α-CD4, α-CD8 antibodies for 15–20 min at RT in dark and then the

cells were fixed in Cytofix and permeabilized with Perm/Wash Buffer using Fixation Permeabilization solution kit (#554714, BD Biosciences). Thereafter, permeabilized cells were used for intracellular cytokine staining by using α-IFN-γ-PE, α-IL17A-PE-Cy7, α-Perforin-APC, α-GzB-FITC, α-IL-4-PE antibodies in permeabilizing buffer in dark for 20 min at RT.

For surface staining only, freshly isolated cells were first blocked with Fc block and then stained directly with desired antibodies. The cells were then washed and analyzed by flow cytometry (Canto II; BD Bioscience). Data analysis was performed using FlowJo software (Tree-Star). For cytokine intracellular staining, cells were stained for surface molecules and then fixated and permeabilized using BD Cyto Fix/ Cyto perm buffer (BD).

Viral load

Homogenized lung samples or thymus cells in Trizol reagent (Invitrogen) were used for RNA isolation as per the manufacturer's protocol. Thereafter, RNA was quantitated by NanoDrop and 1 µg of total RNA was then reverse-transcribed to cDNA using the iScript cDNA synthesis kit (Biorad; #1708891) (Roche). Diluted cDNAs (1:5) were used for qPCR by using KAPA SYBR® FAST qPCR Master Mix (5X) Universal Kit (KK4600) on a Fast 7500 Dx real-time PCR system (Applied Biosystems) and the results were analyzed with SDS2.1 software. Briefly, cDNA was used as a template for the CDC-approved commercial reagent for SARS-CoV-2 N gene: 5'-GACCCCAAAATCAGCGAAAT-3' (Forward), 5'-TCTGGTTACTGCCAGTTGAATCTG-3' (Reverse). Beta-actin gene was used as an endogenous control and was used for normalization through quantitative RT-PCR. The region of N gene of SARS-CoV-2 starting from 28287 – 29230 was cloned into pGEM®-T-Easy vector (Promega). This clone was linearized using SacII enzyme and *in vitro* transcribed using the SP6 RNA polymerase (Promega). The transcript was purified and used as a template for generating a standard curve to estimate the copy number of SARS-CoV-2 N RNA.

Histology

Excised lung or thymus of animals were fixed in 10% formalin solution and processed for paraffin embedding. The paraffin blocks were cut into 2-µm-thick sections and then mounted on silane-coated glass slides. One section from each organ sample was stained with haematoxylin and eosin or for immuno-fluorescence microscopy for N-protein. Stained sections were visualized at 60X magnification and assessment was carried out by blinded trained pathologist by scoring on the scale of 0-5 (where 0 meant no observable pathological feature and score of 5 was given to highest pathological feature.

Immunofluorescence microscopy.

Thin paraffin sections were deparaffinized using xylene, immediately immersed in acetone, rehydrated and washed with ethanol and water subsequently. The antigen retrieval was performed by heating samples to 120 °C for 5 min in citrate buffer (1.8 mM citric acid and 8.2 mM sodium citrate in water) in a 2100 PickCell Retriever (Aptum Biologics). Sections were washed with 1X PBS for 3 times at 5 min each.

Tissue sections were blocked with 5% goat serum in PBS containing 0.05% Tween20 for 1 h at room temperature in a moist chamber. Tissue sections were incubated overnight at 4 °C in a moist chamber with primary antibody used at a concentration of 5ug/ml of SARS-Cov-2 Nucleocapsid diluted in blocking solution. Sections were rinsed three times with PBST at 5 min each and were incubated with secondary antibody for 2 h at RT, and rinsed three times with PBST at 5 min interval. The tissue sections were counterstained with DAPI for 2 min to highlight nuclei and were washed 3 times with PBST at 5 min interval each. The sections were then mounted by using Prolong gold Antifade reagent (Invitrogen). Cells were imaged using a Leica TCS SP8 confocal microscope (Leica Microsystems). Image analysis was performed on the LASX offline analysis software (Leica).

ELISA

Sandwich ELISA was performed for detecting IFN-γ in the BALF samples isolated at end point from mice as previously described [19]. Briefly, coating antibody α-mouse IFN-γ (1:1000 dilution) was coated in carbonate/bicarbonate buffer, pH 9.6 in a 96 well high affinity ELISA plates (Nunc) overnight at 4 °C. 1X overnight at. Next day, 5 % skimmed milk (blocking buffer) was used for blocking and then BALF samples diluted 1:1 was added to each well against a known standard control and incubated at room temperature (RT) for 1 h. Washing was done three times with washing buffer (PBS + 0.05 % tween 20). Thereafter, wells were incubated with biotinylated anti-mouse IFN-γ detection antibody (1:1000 dilution) for 1 h and washed subsequently with washing buffer and incubated further with Avidin-HRP (1:10000 dilution) (Sigma) for 30 min at RT. Thereafter, wells were washed five times and 50 µl of TMB substrate (Thermo Fisher Scientific) was added and incubated in dark for 15-20 min at RT. The reaction was stopped by adding 50 µl of 1 N H_2SO_4 and the plates were read at 450 nm on a 96-well microtiter plate reader. Unknown concentration of IFN-γ was calculated by using calibration curve for IFN-γ standard control.

Statistical analysis

All the results were analysed and plotted using Graph pad prism 7.0 software. Body mass, thymus mass, gene expression, FACS, and ELISA results were compared and analysed using one-way ANOVA or two-way ANOVA or student *t*-test with multiple comparison as mentioned in the legend. Each experiment was repeated 6 times independently. P-value of less than 0.05 and was considered as statistically significant.

Declarations

Acknowledgments

Financial support was provided to the AA laboratory from THSTI core, Translational Research Program (TRP), BIRAC grants (BT/CS0054/21 and BT/CTH/0004/21) Department of Biotechnology (DBT) and DST-SERB. ZAR is supported by intramural funding (THSTI). Immunology Core and FACS facility for providing support in experimentation. We acknowledge SAF and infectious disease research facility (IDRF) for its support. ILBS bio-bank for support in histological analysis and assessment. RCB microscopy facility for microscopic examination of the histology slide. We acknowledge the technical

support of Manas and Sandeep. SARS-CoV-2 and its variants were deposited by the Centres for Disease Control and Prevention and obtained through BEI Resources, NIAID, NIH: SARS Related Coronavirus 2, Isolate USA-WA1/2020, NR-52281.

Author Contributions

Conceived, designed and supervised the study: AA; Designed and performed the experiments: ZAR; ABSL3 experiment: ZAR, SS, JD; FACS: ZAR, SS, JD; qPCR: ZAR; ELISA: ZAR; Fluorescence microscopy: PS, MK; Antibody P4A2: RK; Analyzed the data: ZAR; Contributed reagents/materials/analysis tools: AA; Wrote the manuscript: ZAR, AA.

Declaration of Interests

The authors declare no conflict of interest.

Competing Interests

The authors declare no competing interest.

Materials and correspondence

Correspondence and material request should be addressed to

Amit Awasthi, PhD

Immuno-biology Laboratory,

Translational Health Science & Technology Institute (THSTI)

3rd Milestone, Faridabad-Gurgoan Expressway, Faridabad, Haryana, India 121001

Email: aawasthi@thsti.res.in

Phone: +91-129-287-6482, fax: +91-129-287-6500

References

1. Guan, W.-J. *et al.* Clinical Characteristics of Coronavirus Disease 2019 in China. N Engl J Med **382**, 1708–1720 (2020).
2. Gupta, A. *et al.* Extrapulmonary manifestations of COVID-19. Nat Med **26**, 1017–1032 (2020).
3. Chung, M. K. *et al.* COVID-19 and Cardiovascular Disease. Circulation Research **128**, 1214–1236 (2021).
4. Yang, L. & Tu, L. Implications of gastrointestinal manifestations of COVID-19. The Lancet Gastroenterology & Hepatology **5**, 629–630 (2020).

5. Tan, L. *et al.* Lymphopenia predicts disease severity of COVID-19: a descriptive and predictive study. Sig Transduct Target Ther **5**, 1–3 (2020).
6. Chiang, K., Kalantar-Zadeh, K. & Gupta, A. *Thymic Dysfunction and Atrophy in COVID-19 Disease Complicated by Inflammation, Malnutrition and Cachexia*. https://papers.ssrn.com/abstract=3649836 (2020) doi:10.2139/ssrn.3649836.
7. Liu, B. *et al.* Severe influenza A(H1N1)pdm09 infection induces thymic atrophy through activating innate CD8 + CD44 hi T cells by upregulating IFN- γ. Cell Death Dis **5**, e1440–e1440 (2014).
8. Luo, M., Xu, L., Qian, Z. & Sun, X. Infection-Associated Thymic Atrophy. Frontiers in Immunology **12**, (2021).
9. Savino, W. The Thymus Is a Common Target Organ in Infectious Diseases. PLOS Pathogens **2**, e62 (2006).
10. Elfaki, Y. *et al.* Influenza A virus-induced thymus atrophy differentially affects dynamics of conventional and regulatory T-cell development in mice. European Journal of Immunology **51**, 1166–1181 (2021).
11. Wang, W., Thomas, R., Oh, J. & Su, D.-M. Thymic Aging May Be Associated with COVID-19 Pathophysiology in the Elderly. Cells **10**, 628 (2021).
12. Duan, X. *et al.* NK-cells are involved in thymic atrophy induced by influenza A virus infection. J Gen Virol **96**, 3223–3235 (2015).
13. Vogel, A. B. *et al.* Highly Pathogenic Influenza Virus Infection of the Thymus Interferes with T Lymphocyte Development. The Journal of Immunology **185**, 4824–4834 (2010).
14. Deobagkar-Lele, M., Chacko, S. K., Victor, E. S., Kadthur, J. C. & Nandi, D. Interferon-γ- and glucocorticoid-mediated pathways synergize to enhance death of CD4(+) CD8(+) thymocytes during Salmonella enterica serovar Typhimurium infection. Immunology **138**, 307–321 (2013).
15. Haynes, B. F. *et al.* Analysis of the adult thymus in reconstitution of T lymphocytes in HIV-1 infection. J Clin Invest **103**, 453–460 (1999).
16. Košmrlj, A. *et al.* Effects of thymic selection of the T-cell repertoire on HLA class I-associated control of HIV infection. Nature **465**, 350–354 (2010).
17. Kellogg, C. & Equils, O. The role of the thymus in COVID-19 disease severity: implications for antibody treatment and immunization. Hum Vaccin Immunother **17**, 638–643 (2021).
18. Francis, M. E. *et al.* SARS-CoV-2 infection in the Syrian hamster model causes inflammation as well as type I interferon dysregulation in both respiratory and non-respiratory tissues including the heart and kidney. PLOS Pathogens **17**, e1009705 (2021).
19. Rizvi, Z. A. *et al.* Golden Syrian hamster as a model to study cardiovascular complications associated with SARS-CoV-2 infection. eLife **11**, e73522 (2022).
20. Chan, J. F.-W. *et al.* Simulation of the Clinical and Pathological Manifestations of Coronavirus Disease 2019 (COVID-19) in a Golden Syrian Hamster Model: Implications for Disease Pathogenesis and Transmissibility. Clinical Infectious Diseases **71**, 2428–2446 (2020).

21. Sia, S. F. *et al.* Pathogenesis and transmission of SARS-CoV-2 in golden hamsters. Nature 1–7 (2020) doi:10.1038/s41586-020-2342-5.
22. Winkler, E. S. *et al.* SARS-CoV-2 infection of human ACE2-transgenic mice causes severe lung inflammation and impaired function. Nature Immunology **21**, 1327–1335 (2020).
23. McCray, P. B. *et al.* Lethal Infection of K18-hACE2 Mice Infected with Severe Acute Respiratory Syndrome Coronavirus. Journal of Virology **81**, 813–821 (2007).
24. Schneider, W. M., Chevillotte, M. D. & Rice, C. M. Interferon-stimulated genes: a complex web of host defenses. Annu Rev Immunol **32**, 513–545 (2014).
25. Adamo, S. *et al.* Profound dysregulation of T cell homeostasis and function in patients with severe COVID-19. Allergy **76**, 2866–2881 (2021).
26. Mathew, D. *et al.* Deep immune profiling of COVID-19 patients reveals distinct immunotypes with therapeutic implications. Science **369**, (2020).
27. Barreira-Silva, P. *et al.* IFNγ and iNOS-Mediated Alterations in the Bone Marrow and Thymus and Its Impact on Mycobacterium avium-Induced Thymic Atrophy. Frontiers in Immunology **12**, (2021).
28. Refaeli, Y., Van Parijs, L., Alexander, S. I. & Abbas, A. K. Interferon γ Is Required for Activation-induced Death of T Lymphocytes. J Exp Med **196**, 999–1005 (2002).
29. Moore, J. B. & June, C. H. Cytokine release syndrome in severe COVID-19. Science **368**, 473–474 (2020).
30. Liu, B. *et al.* Anti-IFN-γ therapy alleviates acute lung injury induced by severe influenza A (H1N1) pdm09 infection in mice. Journal of Microbiology, Immunology and Infection **54**, 396–403 (2021).
31. Flerlage, T., Boyd, D. F., Meliopoulos, V., Thomas, P. G. & Schultz-Cherry, S. Influenza virus and SARS-CoV-2: pathogenesis and host responses in the respiratory tract. Nat Rev Microbiol **19**, 425–441 (2021).
32. Bonifacius, A. *et al.* COVID-19 immune signatures reveal stable antiviral T cell function despite declining humoral responses. Immunity **54**, 340–354.e6 (2021).
33. Beigel, J. H. *et al.* Remdesivir for the Treatment of Covid-19 — Final Report. New England Journal of Medicine **383**, 1813–1826 (2020).
34. Wang, Y. *et al.* Remdesivir in adults with severe COVID-19: a randomised, double-blind, placebo-controlled, multicentre trial. The Lancet **395**, 1569–1578 (2020).
35. Geers, D. *et al.* SARS-CoV-2 variants of concern partially escape humoral but not T cell responses in COVID-19 convalescent donors and vaccine recipients. Science Immunology **6**, eabj1750 (2021).
36. McCallum, M. *et al.* Molecular basis of immune evasion by the Delta and Kappa SARS-CoV-2 variants. Science **374**, 1621–1626 (2021).
37. McCallum, M. *et al.* Structural basis of SARS-CoV-2 Omicron immune evasion and receptor engagement. Science **375**, 864–868 (2022).
38. Halfmann, P. J. *et al.* SARS-CoV-2 Omicron virus causes attenuated disease in mice and hamsters. Nature 1–1 (2022) doi:10.1038/s41586-022-04441-6.

39. Kumar, R. *et al.* A broadly neutralising monoclonal antibody overcomes the mutational landscape of emerging SARS-CoV2 variant of concerns. (2022) doi:10.21203/rs.3.rs-1431974/v1.
40. Brouwer, P. J. M. *et al.* Potent neutralizing antibodies from COVID-19 patients define multiple targets of vulnerability. Science **369**, 643–650 (2020).
41. Leng, L. *et al.* Pathological features of COVID-19-associated lung injury: a preliminary proteomics report based on clinical samples. Signal Transduction and Targeted Therapy **5**, 1–9 (2020).
42. Guo Junyi, Huang Zheng, Lin Li, & Lv Jiagao. Coronavirus Disease 2019 (COVID-19) and Cardiovascular Disease: A Viewpoint on the Potential Influence of Angiotensin-Converting Enzyme Inhibitors/Angiotensin Receptor Blockers on Onset and Severity of Severe Acute Respiratory Syndrome Coronavirus 2 Infection. Journal of the American Heart Association **9**, e016219 (2020).
43. Neurath, M. F. COVID-19 and immunomodulation in IBD. Gut **69**, 1335–1342 (2020).
44. Mao, L. *et al.* Neurologic Manifestations of Hospitalized Patients With Coronavirus Disease 2019 in Wuhan, China. JAMA Neurol **77**, 683–690 (2020).
45. Mortaz, E., Tabarsi, P., Varahram, M., Folkerts, G. & Adcock, I. M. The Immune Response and Immunopathology of COVID-19. Front Immunol **11**, 2037 (2020).
46. Egerton, M., Scollay, R. & Shortman, K. Kinetics of mature T-cell development in the thymus. Proc Natl Acad Sci U S A **87**, 2579–2582 (1990).
47. Takaba, H. & Takayanagi, H. The Mechanisms of T Cell Selection in the Thymus. Trends in Immunology **38**, 805–816 (2017).
48. Majumdar, S. & Nandi, D. Thymic Atrophy: Experimental Studies and Therapeutic Interventions. Scandinavian Journal of Immunology **87**, 4–14 (2018).
49. Cullen, S. P. & Martin, S. J. Mechanisms of granule-dependent killing. Cell Death Differ **15**, 251–262 (2008).
50. Dotiwala, F. *et al.* Killer lymphocytes use granulysin, perforin and granzymes to kill intracellular parasites. Nat Med **22**, 210–216 (2016).
51. Cullen, S. P., Brunet, M. & Martin, S. J. Granzymes in cancer and immunity. Cell Death Differ **17**, 616–623 (2010).
52. McGeachy, M. J., Cua, D. J. & Gaffen, S. L. The IL-17 Family of Cytokines in Health and Disease. Immunity **50**, 892–906 (2019).
53. Junttila, I. S. Tuning the Cytokine Responses: An Update on Interleukin (IL)-4 and IL-13 Receptor Complexes. Frontiers in Immunology **9**, (2018).
54. Planas, D. *et al.* Sensitivity of infectious SARS-CoV-2 B.1.1.7 and B.1.351 variants to neutralizing antibodies. Nature Medicine **27**, 917–924 (2021).
55. Thiruvengadam, R. *et al.* Effectiveness of ChAdOx1 nCoV-19 vaccine against SARS-CoV-2 infection during the delta (B.1.617.2) variant surge in India: a test-negative, case-control study and a mechanistic study of post-vaccination immune responses. The Lancet Infectious Diseases **22**, 473–482 (2022).

56. Rizvi, Z. A. *et al.* High-salt diet mediates interplay between NK cells and gut microbiota to induce potent tumor immunity. Sci Adv **7**, eabg5016 (2021).

Figures

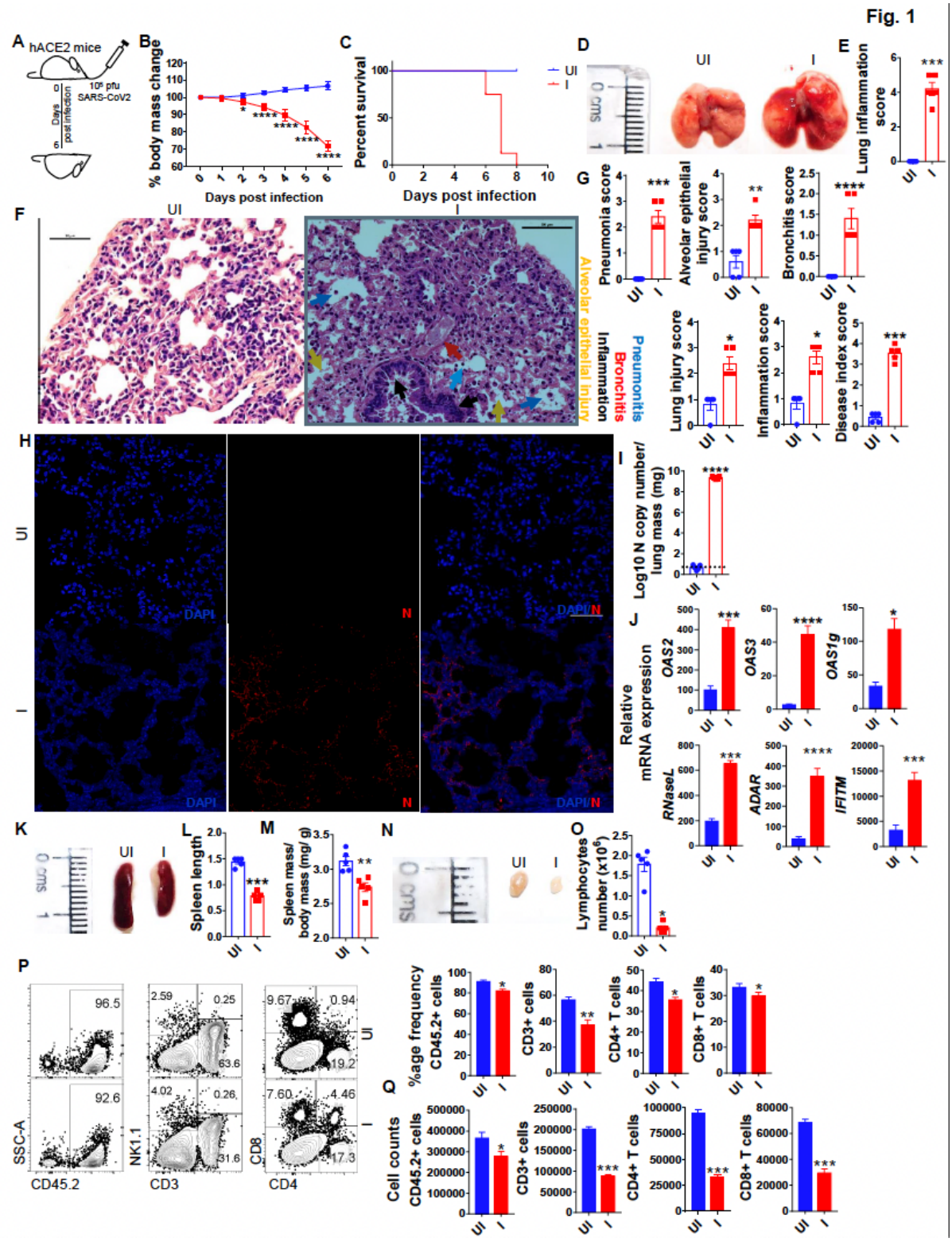

Figure 1

Pulmonary pathology and peripheral lymphocyte profile of SARS-CoV-2 infection in hACE2-Tg mice. Animals intranasally infected with SARS-CoV-2 10^5 pfu/ mice were euthanized on day 6 on the day they become moribund according to the (A) scheme shown. (B) Percentage changes in the body mass of the animals as compared to the day 0 body mass. (C) Percentage of animals surviving plotted against days post challenge. (D) Representative images of the excised lungs and their respective (E-G) inflammation score from excised lungs and H & E stained images (60X) and assessment by blinded trained pathologist on the scale of 0-5, (where 0 means no inflammation and 5 represents maximum score). (H) Immunofluorescence microscopy image of lung section showing SARS-CoV-2 specific N protein (red color), DAPI stain (blue color) and overlay image (DAPI+N protein) acquired at 60X magnification. (I) Lung viral load showing N gene copy number. (J) mRNA expression of anti-viral genes from the lung samples. (K-L) Representative images of excised spleen with respective bar graphs showing (L & M) spleen length and spleen mass/ body mass ratio. (N) Representative images of excised brachial lymph node and its (O) cell count by trypan blue live/dead method. (P-Q) Representative FACS dot plot and its corresponding bar graph showing percentage frequency and (Q) cell count mean $\pm$ SEM of lymphocytes in the spleen. (A-I, K-Q) n=5, (J) n=3. Non-parametric t-test using Mann-Whitney test. *P < 0.05, **P < 0.01, ***P < 0.001, ****P < 0.0001.

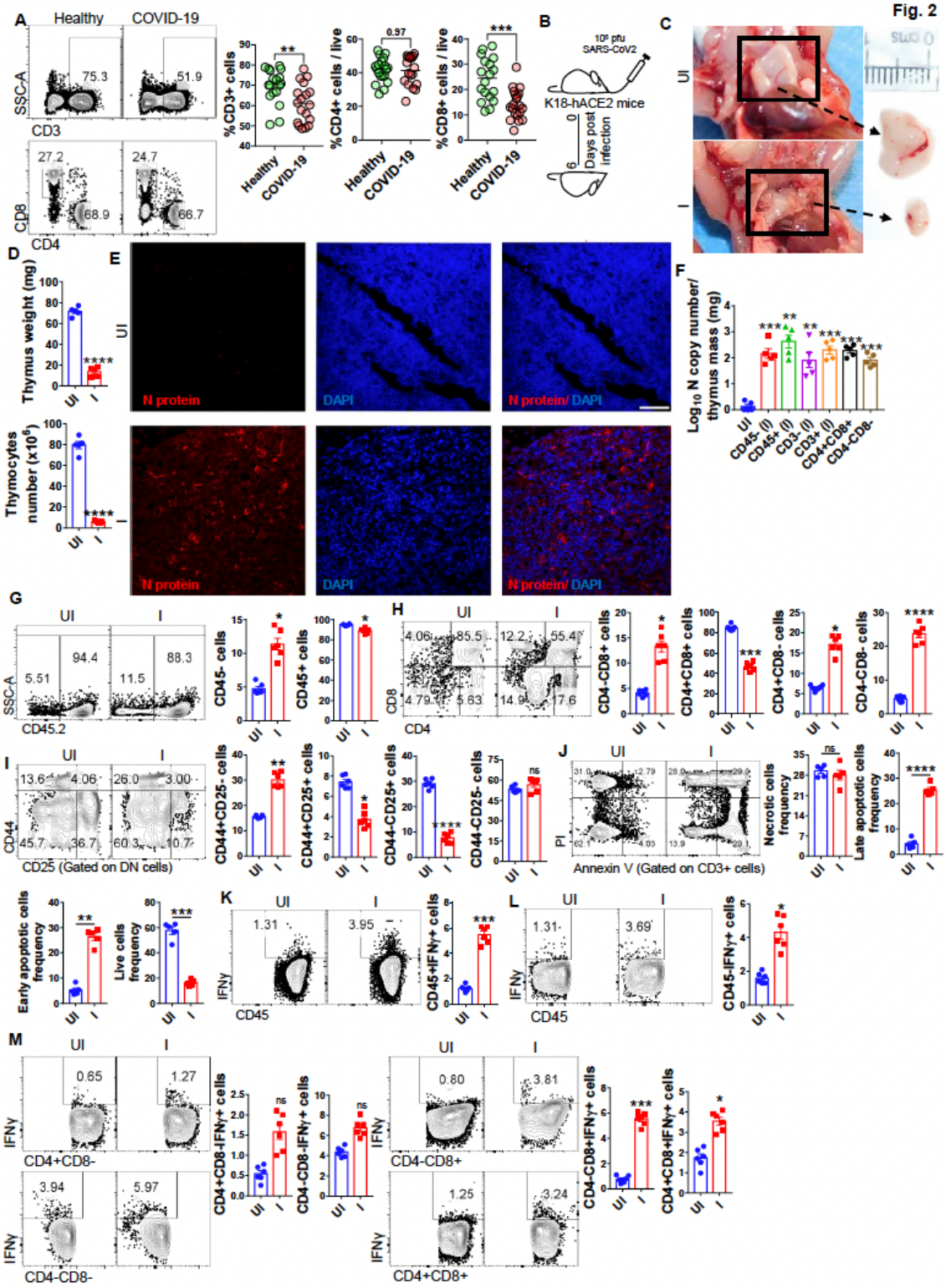

Figure 2

Immuno-pathology of thymus of SARS-CoV-2 infected animals. (A) Immunophenotyping of COVID-19 patients compared to healthy controls (n=18 each). Each dot SSC-A vs CD3, CD4 vs CD8 represents the %frequency of respective cell types per total live cells in PBMCs of an individual subject. Bars represent median values for % CD3 cells/live % CD4 cells/live % CD8 cells/live. **(I-M)** hACE2-Tg mice intranasally (I) infected with 10^5 pfu SARS-CoV-2 were euthanized at the time points indicated and immuno-pathological

changes in the thymus was studied as compared to the uninfected (UI) control. (B) Schematic representation of hACE2-Tg transgenic mice study. The animals were sacrificed on day 6 or on the day they become moribund or otherwise indicated. (C) Representative image of excised thymus along with thymus (D) weight and number. (E) Immunofluorescence microscopy image of thymus section showing SARS-CoV-2 specific N protein (red color), DAPI stain (blue color) and overlay image (DAPI+N protein) acquired at 60X magnification. (F) bar graph showing mean ± SEM of N gene copy for sorted populations of thymus. Representative FACS dot plot and its corresponding bar graph showing percentage frequency mean ± SEM showing (G) SSC-A vs CD45.2 (H) CD4 vs CD8 gated on CD45.2+ cells (I) CD44 vs CD25 gated on DN cells (J) PI vs Annexin V gated on CD3+ cells (K) IFN-γ vs CD45+ (L) IFN-γ vs CD45- and (M) IFN-γ vs different CD4/CD8 sub-populations in the thymus. (D-F) n=5; (B-C, G-M) n=6. Non-parametric t-test using Mann-Whitney test. *P < 0.05, **P < 0.01, ***P < 0.001, ****P < 0.0001.

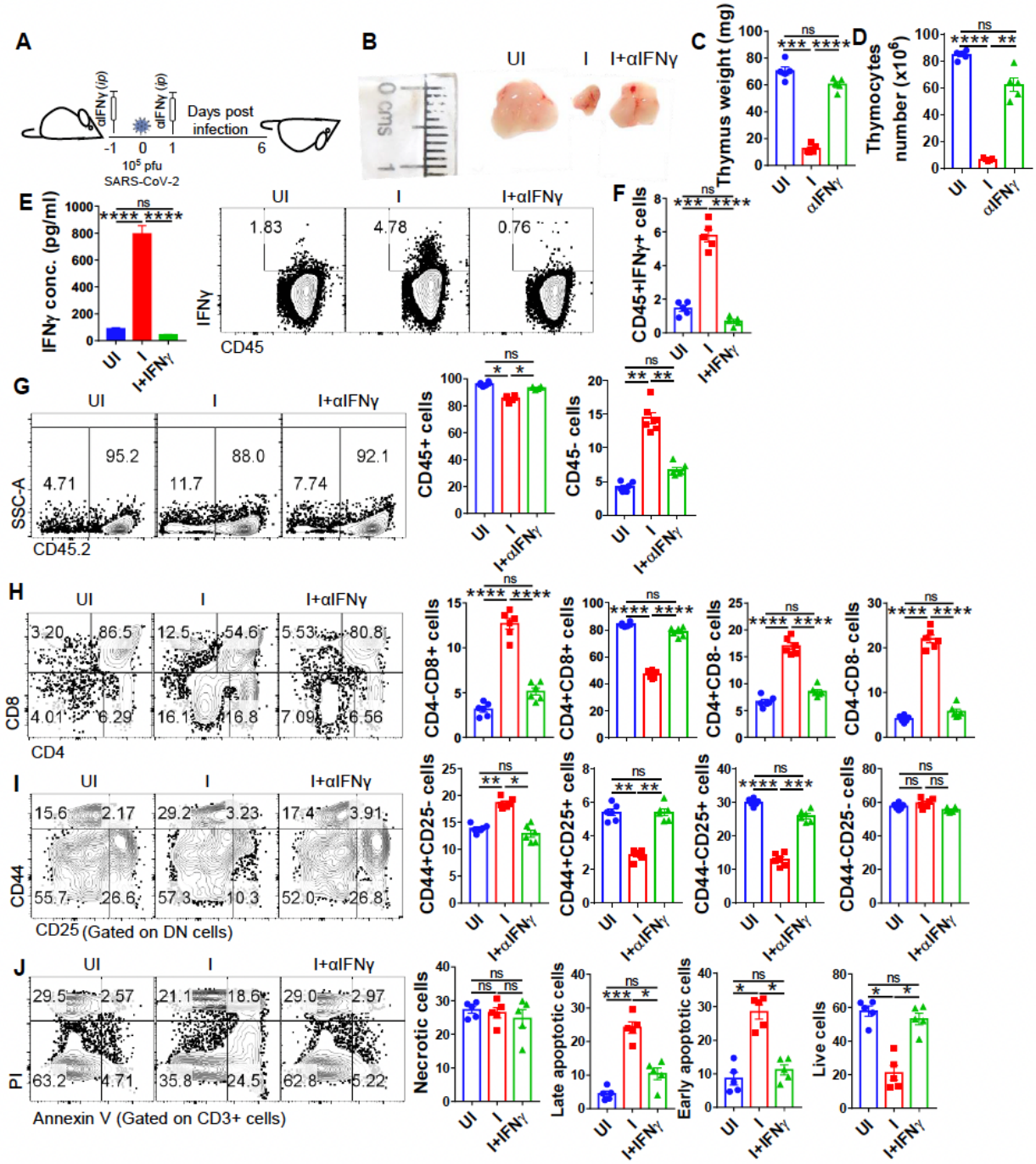

Figure 3

Effect of IFN-γ neutralization on thymic atrophy in SARS-CoV-2 infected hACE2-Tg mice. Neutralizing monoclonal antibody against IFN-γ was used to understand the response of IFN-γ neutralization on thymic atrophy in infected mice. (A) schematic representation indicating schedule for anti-IFN-γ antibody injection. (B) Representative images of excised thymus. (C & D) Bar graph showing mean ± standard error mean (SEM) of thymus wight (mg) and live thymocytes. (E) BALF IFN-γ quantitation by ELISA. Representative FACS dot plot and its corresponding bar graph showing percentage frequency mean ± SEM showing (F) IFN-γ vs CD45 (G) SSC-A vs CD45.2 (H) CD4 vs CD8 gated on CD45.2+ cells (I) CD44 vs CD25 gated on DN cells (J) PI vs Annexin V gated on CD3+ cells in the thymus. (C-E) n=5; (A-B, E-I) n=6.

One way-Anova using non-parametric Kruskal-Wallis test for multiple comparison. *P < 0.05, **P < 0.01, ***P < 0.001, ****P < 0.0001.

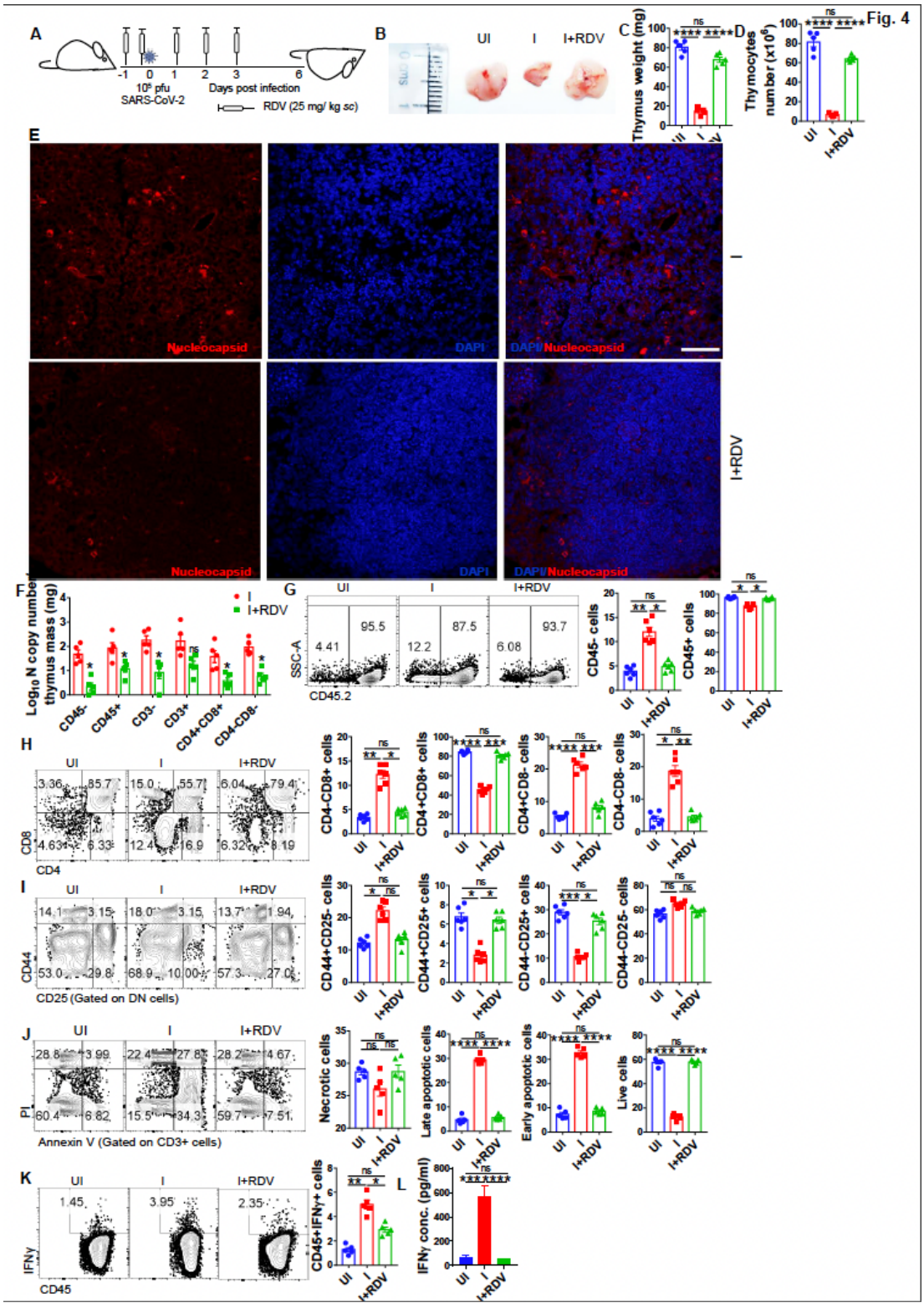

Figure 4

Effect of remdesivir treatment on thymic atrophy in SARS-CoV-2 infected hACE2-Tg mice. Protective efficacy of remdesivir (RDV), used as a prototypic anti-viral drug, against induction of thymic atrophy upon SARS-CoV-2 infection in hACE2-Tg mice. (A) schematic representation showing treatment regime and dose of remdesivir given to SARS-CoV-2 infected mice. (B) Representative images of excised thymus. (C & D) Thymus weight and number shown by bar graph indicating mean ± standard error mean (SEM). (E) Images of immunofluorescence microscopy of thymus section showing SARS-CoV-2 specific N protein (red color), DAPI stain (blue color) and overlay image (DAPI+N protein) acquired at 60X magnification. (F) N gene copy number for sorted thymic populations shown by bar graph mean ± SEM. FACS representative dot plot and its respective bar graph showing percentage frequency mean ± SEM indicating (G) SSC-A vs CD45.2 (H) CD4 vs CD8 gated on CD45.2+ cells (I) CD44 vs CD25 gated on DN cells (J) PI vs Annexin V gated on CD3+ cells (K) IFN-γ vs CD45 in the thymus. (L) Evaluation of IFN-γ from BALF samples by ELISA. (C-F, L) n=5; (A-B, G-K) n=6. One way-Anova using non-parametric Kruskal-Wallis test for multiple comparison. *P < 0.05, **P < 0.01, ***P < 0.001, ****P < 0.0001.

Figure 5

Immuno-pathological changes in thymus infected by SARS-CoV-2 variants. Induction of thymic atrophy in hACE2-Tg mice challenged with SARS-CoV-2 variants such as beta variant (B.1.315), delta variant (B.1.617.2) and omicron variant (B.1.1.529) was studied by intranasal infection 10^5 pfu/ mice followed by euthanization 6 days post infection or on the day when animals became moribund. (A) schematic diagram for VoC challenged hACE2-Tg mice. (B) Representative images of excised thymus. (C & D) Mean

bar graph ± SEM showing thymus wight (mg) and live thymocytes. (E) N gene copy number for sorted thymic populations shown by bar graph mean ± SEM. FACS representative dot plot and its respective bar graph showing percentage frequency mean ± SEM indicating (F) SSC-A vs CD45.2 (G) CD4 vs CD8 gated on CD45.2+ cells (H) PI vs Annexin V gated on CD3+ cells (I) IFN-γ vs CD45 for UI and VoCs in the thymus. (C-E) n=5; (A-B, F-I) n=6. (C-I) One way-Anova using non-parametric Kruskal-Wallis test for multiple comparison. *P < 0.05, **P < 0.01, ***P < 0.001, ****P < 0.0001.

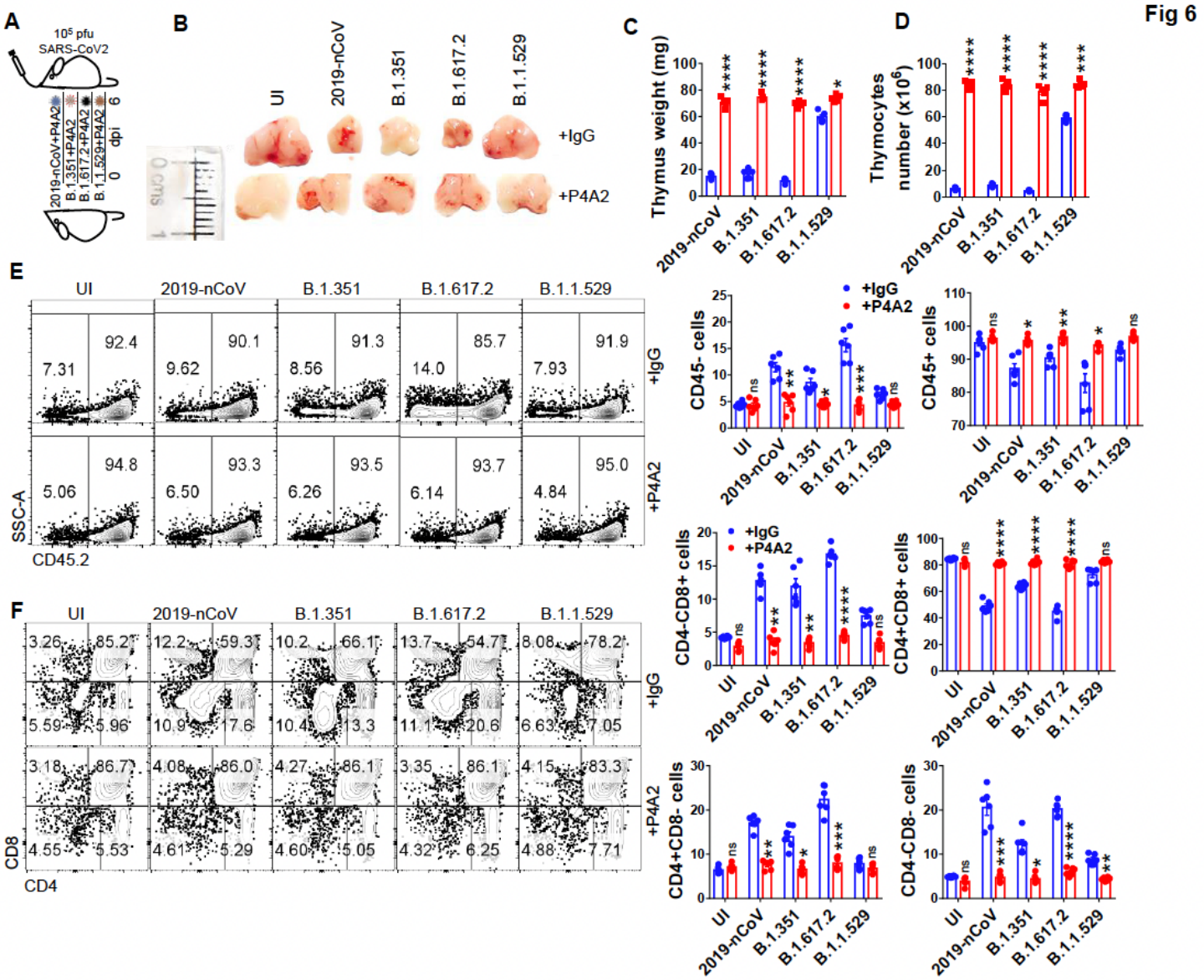

Figure 6

Recovery of thymic atrophy by broadly SARS-CoV-2 neutralizing monoclonal antibody P4A2. Induction of thymic atrophy in hACE2-Tg mice challenged with SARS-CoV-2 variants such as beta variant (B.1.315), delta variant (B.1.617.2) and omicron variant (B.1.1.529) was studied by intranasal infection 10^5 pfu/

mice followed by euthanization 6 days post infection or on the day when animals became moribund. (A) schematic diagram for VoC challenged hACE2-Tg mice. (B) Representative images of excised thymus. (C & D) Mean bar graph ± SEM showing thymus wight (mg) and live thymocytes. (E) N gene copy number for sorted thymic populations shown by bar graph mean ± SEM. FACS representative dot plot and its respective bar graph showing percentage frequency mean ± SEM indicating (F) SSC-A vs CD45.2 (G) CD4 vs CD8 gated on CD45.2+ cells (H) PI vs Annexin V gated on CD3+ cells (I) IFN-γ vs CD45 for UI and VoCs in the thymus. (J-O) Therapeutic efficacy of P4A2 broadly SARS-CoV-2 neutralizing antibody in protecting against thymic atrophy by SARS-CoV-2 variants. (J) IFN-γ ELISA from BALF samples. (K) Scheme for VoC challenge in presence or absence of P4A3. (L) Representative image of excised thymus along with (M) thymus weight and (N) number. Representative FACS dot plot and its corresponding bar graph showing percentage frequency mean ± SEM for VoC thymus in presence or absence of P4A2 (O) SSC-A vs CD45.2 (P) CD4 vs CD8 gated on CD45.2+ cells in the thymus. (C-E, J, L-N) n=5; (A-B, F-I, K-L, O-P) n=6. (C-I) One way-Anova (L-O) Two-way Anova using non-parametric Kruskal-Wallis test for multiple comparison. *P < 0.05, **P < 0.01, ***P < 0.001, ****P < 0.0001.

Supplementary Files

This is a list of supplementary files associated with this preprint. Click to download.

- Supplemenmaterials21042022.pdf